Inflight Calibration of SPOT CCD Detector Geometry

Torbjörn Westin
SSC Satellitbild, Box 861, S-98128 Kiruna, Sweden

ABSTRACT: The fact that the SPOT satellites carry two independent instruments offers a unique possibility to determine the detector position errors in the CCD arrays. By simultaneously imaging the same area with the panchromatic sensors in both instruments, detector errors in one instrument can be measured by comparison with the image from the other instrument. By repeating this measurement in other image pairs, with different displacements between images, a unique solution for the detector position errors in both instruments can be obtained. A method based on generalized inverse algebra is developed for this type of computation, and applied to the SPOT-1 satellite. The results can be used for correcting SPOT scenes for the effects of these errors. This is verified in a test, where systematic errors were successfully eliminated from a DTM computed from a SPOT stereo pair.

INTRODUCTION

DURING THE LAST DECADES, different satellite sensors have emerged as alternatives to photographic cameras in small scale mapping. The development trend towards higher spatial resolution has increased their usefulness. Today, images from the SPOT satellite have a potential to meet geometrical accuracy standards for 1:50,000-scale mapping, both in planimetry and altimetry. Successful exploitation of the high accuracy potential depends on good mathematical models for the viewing geometry, including both exterior and interior orientations. While the calibration of interior orientation elements in mapping cameras is common practice, little attention has been paid to the corresponding problems in satellite sensors. The type of elements to calibrate varies in different types of sensors. In sweep scanners, the mirror scan profile can be considered as an interior orientation element. Instruments with CCD arrays are more similar to cameras, but introduce the positions of individual detectors as a new type of interior orientation element. The purpose of this paper is to develop a method for calibrating detector positions in the SPOT satellites, and to apply it to the panchromatic arrays in the SPOT-1 satellite.

THE SPOT-1 DETECTOR ASSEMBLY

The SPOT-1 satellite has two independent and identical instruments, called HRV1 and HRV2 (HRV = High Resolution Visible). Each instrument operates in two separate modes, panchromatic (P) or multispectral (XS). The XS mode registers light in three narrow bands (green, red, and near IR) at a nominal ground resolution of 20 m. The P mode registers light in one broader band (green to red) at a 10-m resolution. Spectral separation of the four channels is achieved by a focal plane spectral beamsplitter, made of glass prisms with faces covered by dichroic layers.

The imaging is based on the "pushbroom" technique, where one image line is registered simultaneously by 6000 detectors in four CCD arrays. The P line thus comprises 6000 pixels, while the XS line only comprises 3000 pixels because it utilizes two elementary detectors per pixel. The detector array for each spectral band is formed by four separate 1728-point CCD arrays, using 1500 detectors from each (Figure 1). The nominal inter-detector distance is 13 μm. The four CCD arrays cannot be placed edge-to-edge without serious discontinuities in inter-detector distance at the array joints. To overcome this problem, the four CCD arrays were glued on the faces of an optical divider, called DIVIOLI (Figure 2). Here, the positions of the CCD arrays could be adjusted to form a continuous virtual line of high accuracy.

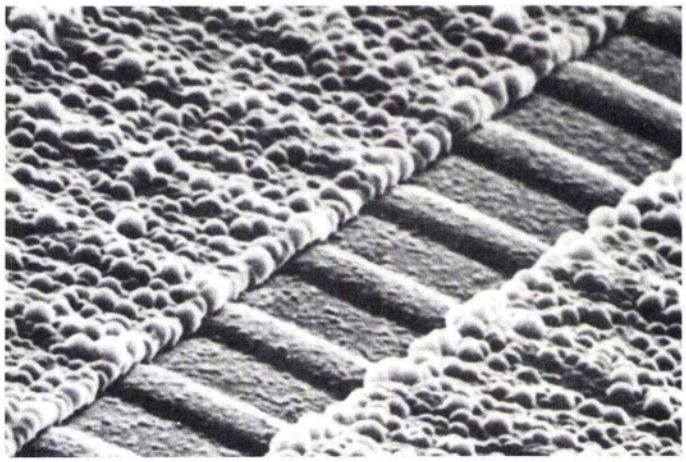

FIG. 1. Enlargement of a small portion of a CCD array, showing about seven individual detectors. (Courtesy of SODERN, contractor for the SPOT camera detection system.)

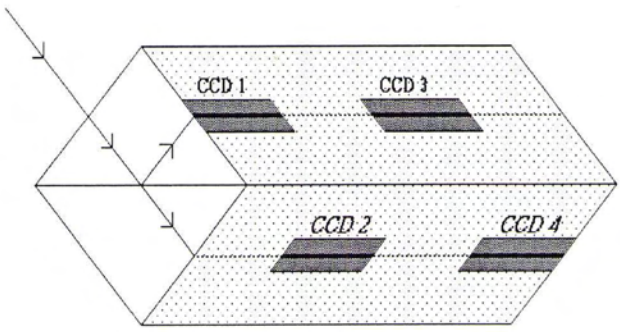

FIG. 2. The DIVIOLI.

PREFLIGHT CALIBRATION RESULTS

The detector position accuracy achieved in preflight tests was reported by Midan (1986) as

Maximum detector offset from nominal position	3μm.

Henry *et al.* (1988) reported the preflight results as

Detector line transverse straightness	±2 μm

PHOTOGRAMMETRIC ENGINEERING & REMOTE SENSING,
Vol. 58, No. 9, September 1992, pp. 1313–1319.

0099-1112/92/5809–1313$03.00/0

Detector line axial straightness	±5 μm
Detector superposition at array joints	±1 μm

(without giving any exact explanation of what was meant by straightness). These errors are large enough to have a significant effect on some image processing operations, especially DTM extraction from stereo pairs. An inflight calibration is thus warranted for two reasons. First, the errors may have changed to the worse due to the launching and space environment. Second, a detailed mapping of the errors along the arrays can be used to correct the final image during resampling.

INFLIGHT MEASUREMENT OF DETECTOR POSITION ERRORS

To construct a test field with three-dimensional targets would clearly be very difficult due to the size of a SPOT scene and the size of the targets necessary to be visible. One possible approach would be to use analytical calibration with ordinary control points. This would, however, have to involve the measurement of many thousands of very exact control points, to be able to measure the possible irregular errors at the one-tenth of a pixel size level in the 6000 detectors of one instrument.

The approach chosen here takes advantage of the fact that it is possible to image the same area at the same time with both instruments on SPOT. The image pair can then be thought of as a stereo pair with a base-to-height ratio equal to zero. Then, if we still find a difference (parallax) between the two images at a given point, it will be a direct measure of the sum of the position errors in the detectors imaging that point in the respective instruments. By repeating these measurements in more than one image pair, with different displacements between images, it is possible to solve for the detector position errors in each separate instrument.

Only the panchromatic sensor is treated in this study. The position errors in the XS sensor are of less importance due to its double pixel size, causing their relative effect to be only half as large as in the P sensor.

DATA SET

Three image pairs were used for the computations. They were chosen from three different years (1987–89), to be able to detect any time variation, and from three different areas, to avoid systematic errors induced by scene content. The needed variation in displacement between images in the pair was achieved by using different viewing directions in each instrument, made possible by the steerable mirrors. The differences in viewing angle were 0.3°, −0.3°, and −0.9° for each pair, respectively.

PREPROCESSING

The two images in a pair cannot be compared unless they are first transformed to a common coordinate system. Here, UTM was used as a reference system. For the orientation process, a satellite model with seven parameters (four orbit and three attitude) was used. A detailed description of this model can be found in Westin (1990). The orientation was done in two steps:

(1) Exterior orientation. The exterior orientation parameters for the HRV1 images from each image pair we were determined using only *a priori* orbit and attitude data. As the ground elevations were unknown, the images were projected onto the ellipsoid during rectification to the UTM system.

(2) Relative orientation. A large number of high contrast, 32- by 32-pixel subimages were extracted from the rectified HRV1 scenes to be used as control points in the modeling of the parameters for the HRV2 scenes. The subimages were assigned coordinates according to the UTM systems in the HRV1 scenes. Automatic correlation was used to find the control point positions in the HRV2 scenes. In modeling the HRV2 scenes, the orbit parameters were constrained to be equal to those in their corresponding HRV1 scenes (the small distance between the two instruments on the satellite can be neglected). Only the three attitude parameters were allowed to vary, to account for deviations from the nominal pointing directions in the instruments. The HRV2 images were finally rectified to the UTM system, using the ellipsoid as reference surface as was done with the HRV1 scenes. The RMS residual errors were close to 0.1 pixel in all three scene-to scene models.

Using the ellipsoid as the projection surface instead of the real ground surface during rectification poses no problem. As the images in a pair were acquired from the same orbital positions, the terrain induced distortions in UTM coordinates are identical in both images, thereby not affecting the difference measurements.

DETERMINATION OF RELATIVE FOCAL LENGTH

The two instruments, HRV1 and HRV2, have separate optical assemblies. The focal length of each instrument is indirectly given in the auxiliary information on the SPOT CCT, by means of the viewing directions for the first and last detector in the line. Assuming the nominal 13-μm inter-detector distance, the focal lengths become

$$f_{HRV1} = 1084.49 \text{ mm}$$
$$f_{HRV2} = 1084.12 \text{ mm} = 0.999659\, f_{HRV1}$$

These are the values from the prelaunch calibrations, and they may have changed. A small error in the focal length is of little importance in normal modeling of one scene, because it will be absorbed in the orbit position parameters. In this case, however, where both images are obtained from the same orbital position, different errors in focal length will cause different scales along a line in the two images. This will directly affect the determination of detector position errors.

The absolute sizes of HRV focal lengths can hardly be calculated with enough precision from inflight measurements. They are however, not of particular interest here. Only variations in the relation between the two focal lengths will introduce distortions. The difference in focal length was determined in conjunction with the preprocessing. The HRV1 instrument was assumed to have an error free focal length, while the value for HRV2 was determined in relation to HRV1. This was accomplished by performing the preprocessing step 2 above twice. First, the HRV2 focal length was treated as a parameter, giving three estimates whose average was

$$f_{HRV2} = 1084.20 \text{ mm} = 0.999733\, f_{HRV1}$$

Now step 2 in the preprocessing could be repeated for all pairs with the new value implemented.

MEASUREMENT OF SCENE-TO-SCENE DIFFERENCES

To be able to extract the differences with high accuracy, software primarily intended for automatic stereo matching of digital SPOT scenes was used. The procedure used, multi-point matching, is based on global least-squares matching of the image pair. The parameters of the resulting DTM are the nodes of a bilinear finite element grid. The details of the matching method can be found in Rosenholm (1987).

The program was set up to calculate the parallaxes in units of 0.01 pixel. For each scene pair, two runs were made, one calculating parallaxes in the line direction, and the other the parallaxes perpendicular to the line direction. In this way, the parallaxes will represent the sum of the detector position errors along or across the CCD arrays. The grid distance in the computation was 200 m (corresponding to 20 detectors).

The resultant grid of differences can be represented by an image, in which lighter pixels represent scene positions with a positive difference, and darker pixels positions with negative difference. Figure 3 shows an example of an along line parallax

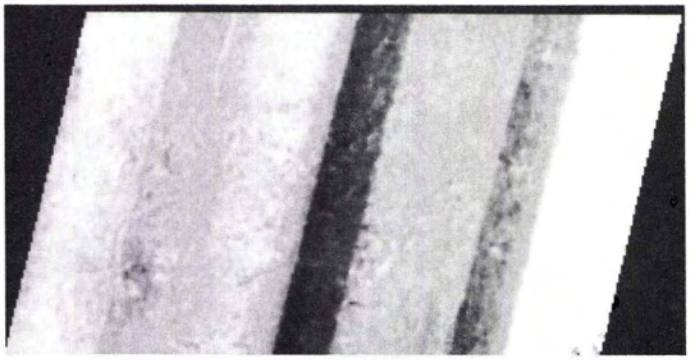

FIG. 3. Difference image for the along-line direction in the first image pair.

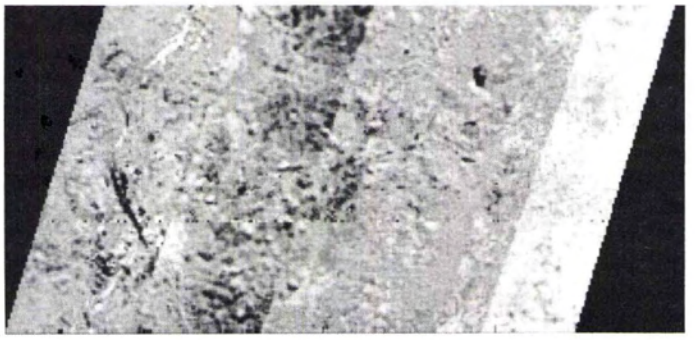

FIG 4. Difference image for the across-line direction in the second image pair.

image, and Figure 4 shows an example of an across line parallax image. Note how clearly the misalignments between the separate CCD arrays in a line show up as a discontinuities in differences. The image also visualizes the distribution of errors that would affect a DTM calculated with this particular overlap between images in the stereo pair.

REDUCTION OF MEASUREMENTS TO THE CCD ARRAYS

The grid of differences was then transformed back to the raw image space of the HRV1 scene. The x-dimension (line direction) of the grid gives the difference as a function of detector number in HRV1. As there is a constant shift between HRV1 and HRV2, we also know it as a function of detector number in HRV2. By averaging the 151 lines in the grid, we finally get an estimate of the difference at each 20th detector, as well as the standard deviation in that estimate.

Examples of these results are shown in Figure 5 for differences in the line direction, and in Figure 6 for across line differences. The positions for CCD array joints are marked as vertical lines in the figures. The misalignments at the joints show up clearly, but it is also obvious that there are other detector position errors, within the separate arrays, which are contributing to the result. This can be seen by the non-linear behavior of differences between joints.

FORMATION OF OBSERVATION EQUATIONS

If misalignments in the CCD array joints had been the only errors, it would have been enough to measure one image pair. Then the size of the jump in the difference function at a joint gives directly the size of the misalignment at that joint in the direction of measure. Now, as there are obviously other errors present, we need more than one image pair to be able to solve for a more detailed distribution of errors.

It would be impossible to solve for the errors for each individual detector. Measurements of differences between images cannot be done on a pixel by pixel basis. A window of some size is required for matching, which will always cause averaging of the individual errors. Choosing a smaller or larger window in matching is a tradeoff between resolution and low variance in our error estimates. As the errors were assumed to vary only slowly over the arrays, a comparatively large window size of 20 detectors were chosen. This also means that the size of the equation systems is kept to manageable sizes, still keeping 600 parameters per direction of measure.

The parameters we want to solve for are

$X1(i)$ = along line error in HRV1 detector group i,
$X2(i)$ = along line error in HRV2 detector group i,
$Y1(i)$ = across line error in HRV1 detector group i, and
$Y2(i)$ = across line error in HRV2 detector group i

for

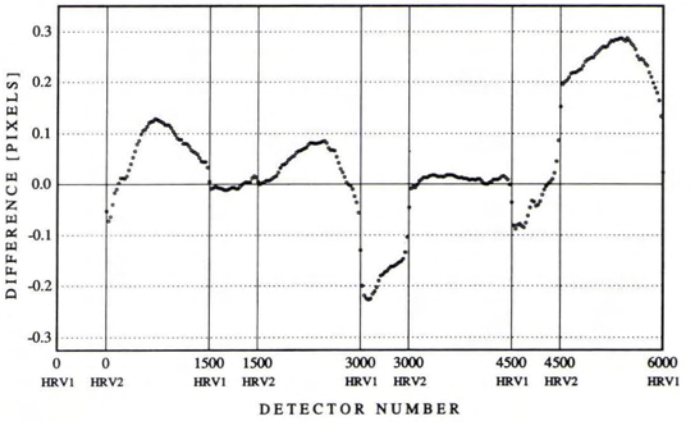

FIG. 5. Measured differences in the along-line direction in the first image pair (corresponding to Figure 3).

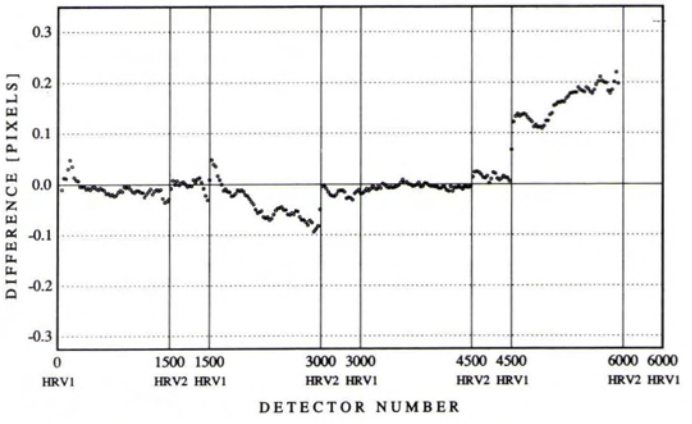

FIG. 6. Measured differences in the across-line direction in the second image pair (corresponding to Figure 4).

$$i = 1...300$$

and each detector group consisting of 20 detectors, making a total line length of 300 by 20 = 6000 detectors.

We can relate our observations to the parameters in equations as follows:

$$X1(i) - X2(i+\Delta_j) = DX_j(i) \quad (1)$$

$$Y1(i) - Y2(i+\Delta_j) = DY_j(i) \quad (2)$$

where

i = HRV1 detector group number,
j = image pair number,
Δ = detector group offset between HRV1 and HRV2,
$DX(i)$ = measured difference in line direction, and
$DY(i)$ = measured difference across line direction.

The **X** and **Y** parameters are solved separately but in an identical way. In the following, only the **X** solution will be discussed.

The Equations 1 can be collected into systems

$$\mathbf{A}_j\mathbf{X} = \mathbf{I}_j \tag{3}$$

and

$$\mathbf{A}\,\mathbf{X} = \mathbf{L} \tag{4}$$

where

$\mathbf{A}_j$ = the $(m_j \times n)$ coefficient matrix for image pair number j,
$\mathbf{L}_j = DX_j$, and

$$\mathbf{A} = \begin{bmatrix} \mathbf{A}_1 \\ \vdots \\ \mathbf{A}_k \end{bmatrix}, \mathbf{X} = \begin{bmatrix} X1 \\ X2 \end{bmatrix}, \mathbf{L} = \begin{bmatrix} \mathbf{L}_1 \\ \vdots \\ \mathbf{L}_k \end{bmatrix} \tag{5}$$

with

k = the number of image pairs used in the solution,
$m = m_1 + \ldots + m_k$ = number of observations, and
$n = n_1 + n_2$ = number of parameters.

If $k=1$, the system is consistent but very much underdetermined (Rank(A) $<n/2$, $m < n/2$). Whatever function X1 we chose, we can always find a function X2 which satisfies Equation 4.

If $k=2$, the system is still consistent and slightly underdetermined (Rank(A) $< n$, $m<n$). It will always be underdetermined, because the scene displacement causes the number of observations for each image pair to always be less than the number of detectors (or detector groups). Here we can get a useful result by a minimum norm solution of the system (Equation 4). There are, of course, an infinite number of solutions but, as will be discussed below, there are reasons to believe that the minimum norm solution should be a good choice. The problem here is that the solution will fit the measurements exactly. If the measured data were not caused by time-constant detector errors, but somehow scene dependent or time variant, they would still give a solution, and we would be left uncertain of its validity.

If $k=3$, the system is overconstrained but still slightly underdetermined (Rank(A) $< n$, $m>n$). If we kept on adding even more image pairs, the system would always be underdetermined. But, as the system now is overconstrained, scene-dependent effects in the measurements will show up in the residuals of a least-squares adjustment, instead of directly affecting the parameters. There is, however, still an infinite number of solutions satisfying the least-squares condition, but we will find good reasons for choosing the minimum norm least-squares solution.

THE SPACE SOLUTIONS

As discussed above, there will always be an infinite number of least-squares solutions to the system (Equation 4). We can illustrate this for the case of two image pairs ($k=2$). Let us first rewrite Equation 1:

$$(X1_t(i) + X1_0(i)) - (X2_t(i+\Delta_1) + X2_0(i+\Delta_1)) = DX_1(i) \tag{5}$$

$$(X1_t(i) + X1_0(i)) - (X2_t(i+\Delta_2) + X2_0(i+\Delta_2)) = DX_2(i) \tag{6}$$

where $X1_t$ and $X2_t$ is the "true" solution to the system (Equation 4), and $X1_0$ and $X2_0$ are any functions that, due to the rank deficiency, can be added to $X1_t$ and $X2_t$ under consistency of the system (Equation 4). While $X1_t$ and $X2_t$ can take any form, $X1_0$ and $X2_0$ must satisfy

$$X1_0(i) = X2_0(i+\Delta_1) \tag{7}$$

$$X1_0(i) = X2_0(i+\Delta_2) \tag{8}$$

which means that both $X1_0$ and $X2_0$ must be periodic with the period $P = |\Delta_1 - \Delta_2|$. The complete set of consistent solutions can then be written:

$$X1(i) = X1_t(i) + a_0 + \sum_{j=1}^{[P/2]} a_j \sin\left(\frac{j2\,\pi i}{P} + \varphi_j\right) \tag{9}$$

$$X2(i) = X2_t(i) + a_0 + \sum_{j=1}^{[P/2]} a_j \sin\left(\frac{j2\pi(i - \Delta_1)}{P} + \varphi_j\right) \tag{10}$$

(where $\varphi_{P/2} = \pi/2$ if P is even).

If we extend our measurements to three image pairs, exactly the same space of periodic solutions will still be present. This is due to the fact that the displacement between images is a function of the instrument mirror angle, and the mirror angle is only incremented in fixed steps of 0.6°. The difference in displacement, the period P, will thus always correspond to a multiple of 0.6° mirror angle.

From this we can draw two conclusions:

- It is not very plausible that the solution should include a function of period P. This periodicity would have to be continuous over the CCD array joints, and would also have to be identical but displaced by Δ_1 in the second instrument. This seems very improbable to happen with eight independently manufactured CCD arrays.
- If the assumption in the previous conclusion holds, then the minimum norm solution will be very close to the "true" solution (X_t).

The reason for only being very close to, and not exactly equal to, the "true" solution is due to the aliasing effects caused by the finite interval the functions are defined on. If the line length had been a multiple of P, the minimum norm solution would have completely eliminated all functions of period P (i.e., $a_j=0$ for $j=0. \ldots [P/2]$). In reality, it is not a multiple of P. This causes the different j-terms in Equations 9 and 10 to no longer be completely orthogonal to each other or to X_t. The minimum norm solution will then result in small, but finite, loads on the coefficients a_j. But as P is small in relation to the total interval n, the deviation will be insignificant compared to other errors caused by imperfect measurements.

NUMERICAL SOLUTION TO THE SYSTEM

The weighted minimum norm least squares solution to Equation 4 is (Bjerhammar, 1971)

$$\mathbf{X} = (\mathbf{A}^T\mathbf{W}\mathbf{A})^g\,\mathbf{A}^T\mathbf{W}\mathbf{L} \tag{11}$$

where $\mathbf{A}^g$ is the generalized inverse satisfying

$$\begin{aligned} \mathbf{A}\mathbf{A}^g\mathbf{A} &= \mathbf{A} \\ \mathbf{A}^g\mathbf{A}\mathbf{A}^g &= \mathbf{A}^g \\ \mathbf{A}\mathbf{A}^g &= (\mathbf{A}\mathbf{A}^g)^T \\ \mathbf{A}^g\mathbf{A} &= (\mathbf{A}^g\mathbf{A})^T \end{aligned} \tag{12}$$

The weight matrix **W** was calculated from the standard deviations in the averages of the 151 lines in the measurement grid. Solving the system was achieved by Cholesky triangular decomposition. But, as $\mathbf{A}^T\mathbf{W}\mathbf{A}$ is rank deficient, a modified version for the semidefinite case with symmetric pivoting had to be used (Golub *et al.*, 1989). A reduced version (**T**) of the triangular result matrix is then constructed by excluding all lines where the diagonal element is zero, due to the rank deficiency. Determining which elements are zero due to rank deficiency

can be a major numerical problem, but as the rank could be calculated from the period P, the number of lines to be excluded was given. The reduced $\mathbf{T}$ still satisfies

$$\mathbf{T}^T\mathbf{T} = \mathbf{A}^T\mathbf{W}\mathbf{A} \quad (13)$$

Bjerhammar (1971) has shown that the weighted minimum norm least-squares solution now is given by

$$\mathbf{X} = \mathbf{T}^T(\mathbf{T}\mathbf{T}^T)^{-1}(\mathbf{T}\mathbf{T}^T)^{-1}\,\mathbf{T}\mathbf{A}^T\mathbf{W}\mathbf{L} \quad (14)$$

which is solvable as the matrix $\mathbf{T}\mathbf{T}^T$ is of full rank.

RESULTS

As mentioned above, three image pairs were used for the computations. The solutions for the X and Y displacement parameters in HRV1 and HRV2, respectively, are given in Figures 7, 8, 9, and 10. The results can be summarized as

Along line maximum offset	0.22 pixels	(2.9 μm)
Along line RMS offset	0.09 pixels	(1.2 μm)
Along line error range	0.39 pixels	(5.1 μm)
Across line maximum offset	0.20 pixels	(2.6 μm)
Across line RMS offset	0.05 pixels	(0.6 μm)
Across line error range	0.28 pixels	(3.6 μm)
Maximum superposition error at array joints	0.11 pixels	(1.4 μm)

where the error range is the difference between the maximum and minimum signed deviations from nominal positions.

The least-squares fit is good, and the estimated standard deviation in the parameters is only around 0.02 pixels, or 0.26 μm. These values are, however, based on the ideal assumption that the measurements were all independent (only a diagonal $\mathbf{W}$ was used), and a possible correlation between neighboring detectors would in reality increase these values somewhat. Figures 11 and 12 show the estimated standard deviations in the parameters as a function of detector number. (The larger values at the edges are due to fewer observations close to the image borders. The regular "notches" are also caused by this border effect, being

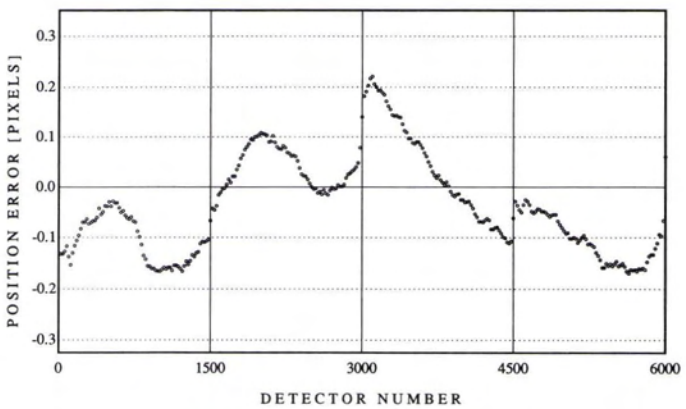

FIG. 7. Detector along-line position errors in HRV1.

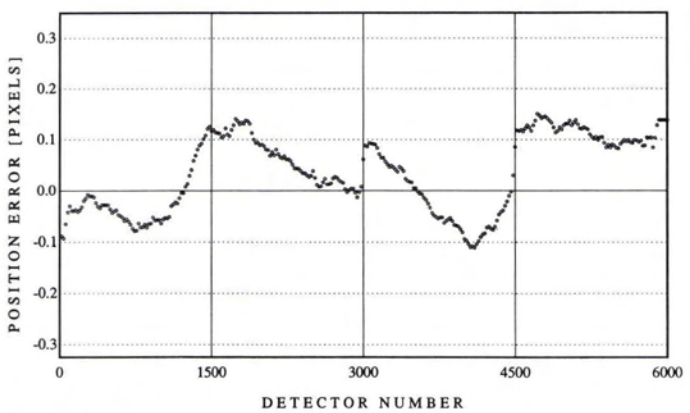

FIG. 8. Detector along-line position errors in HRV2.

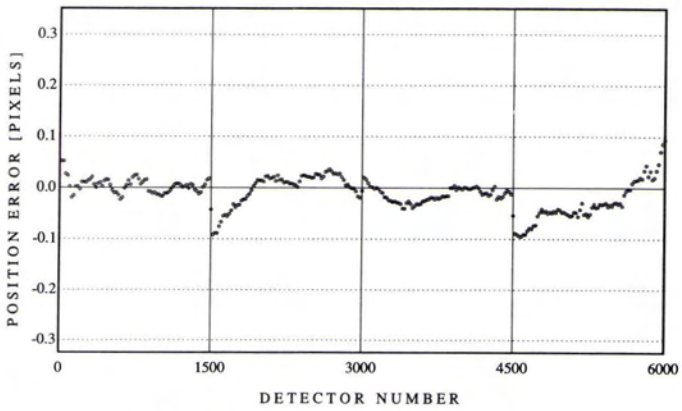

FIG. 9. Detector across-line position erros in HRV1.

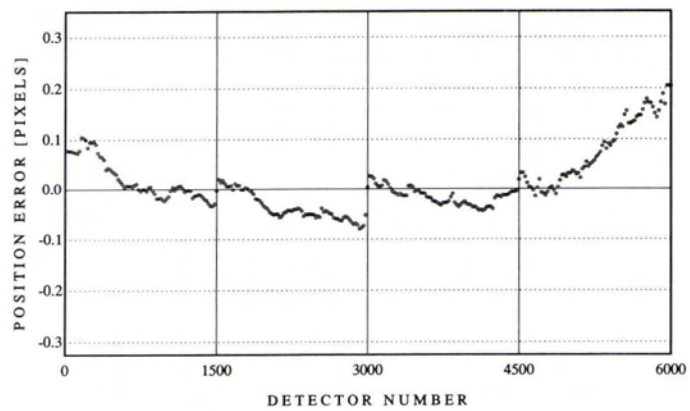

FIG. 10. Detector across-line position errors in HRV2.

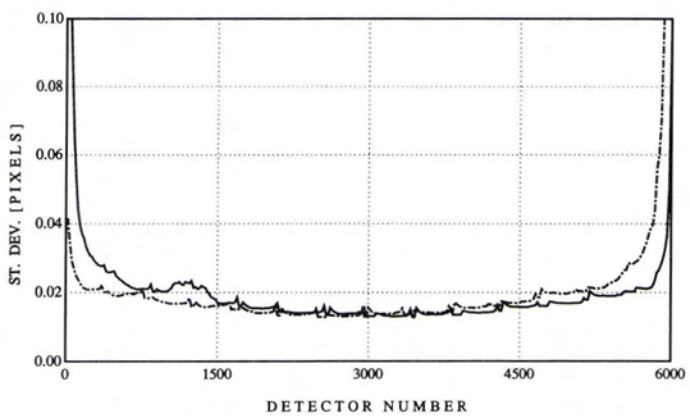

FIG. 11. Estimated standard deviation in along-line errors. The solid line shows HRV1, and the dotted line HRV2.

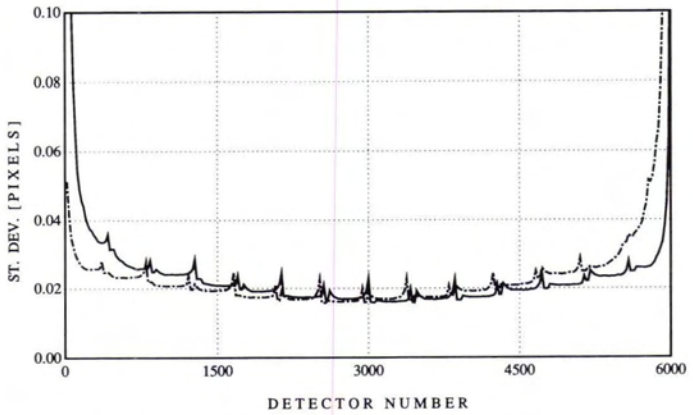

FIG. 12. Estimated standard deviation in across-line errors. The solid line shows HRV1, and the dotted line HRV2.

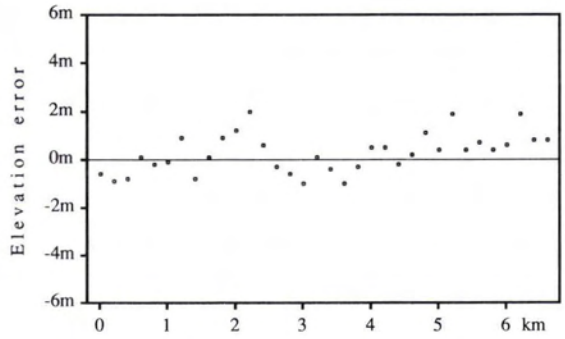

FIG. 13. Difference between the computed DTM (with detector position corrections) and the reference DTM as a function of detector number. A 5-m bias has previously been subtracted from the measured values.

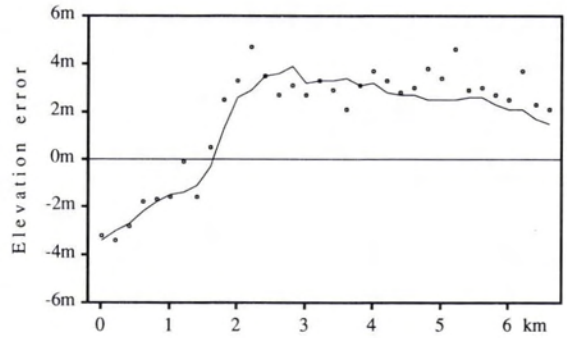

FIG. 14. Difference between the computed DTM (without detector position corrections) and the reference DTM as a function of detector number. A 5-m bias has previously been subtracted from the measured values. The solid line is the errors predicted from the solution of detector offsets.

transported inwards by a cyclic correlation between the parameters.)

The size of the displacements, especially in the along line direction, are large enough to introduce significant errors in the elevations of a DTM, computed from a SPOT stereo pair. The largest elevation error corresponds to the along-line error range of 0.39 pixels, which is much larger than the 0.15 to 0.20-pixel accuracy possible in the stereo matching (Rosenholm, 1988). It would introduce an elevation error of 10 m at a base-to-height ratio of 0.4. Also, the across line offsets introduce errors in the DTM at places where the dominant feature is oblique to the column direction. This may, for example, introduce varying systematic errors in the elevation of a river, depending on its direction of course.

It should be emphasized that the detector position errors in the x direction are correlated to the focal length chosen for HRV2. It is impossible to distinguish between an error in the focal length and a linear trend in the position errors. The results in Figures 7 and 8 are thus only valid for $f_{HRV2} = 0.999733\, f_{HRV1}$. For a satellite model where $f_{HRV1} = f_{HRV1}$, or $f_{HRV2} = 0.999659\, f_{HRV1}$, new parameters in the x direction can be computed by introducing a linear trend in the error function.

IMAGE CORRECTION TEST

The detailed description of detector positions acquired in the solution can be used to correct the satellite image during resampling. This was implemented in the system described in Westin (1990). To check both the correctness of this implementation, and the validity of the position parameters achieved in the solution, a test with stereo processing of SPOT images was performed.

As reference, a DTM provided by the National Swedish Land Survey was used. It had a grid distance of 50 m and an estimated RMS error of 2 m in elevation. Over this area, a SPOT stereopair was acquired. The left image was registered by HRV2 at an angle of 1.4°, while the right was registered by HRV1 at the angle −18.8° (corresponding approximately to a B/H of 0.4). The pair was resampled twice, with and without detector position corrections. Both pairs were then processed in the stereo matching system (Rosenholm, 1988), and the results were compared with the reference DTM. The differences were first averaged along the satellite track to give the differences as a function of detector number. The result for the detector position corrected image pair is shown in Figure 13. The result for the uncorrected pair is given in Figure 14 together with the errors predicted from the knowledge of the detector positions. A constant bias of 5m, which is assumed to have been introduced by errors in the relative orientation of the stereopair, was first subtracted from both results (the same control points were used for both stereopairs, which should cause the bias to be same).

The results in Figure 14 show a good correspondence with the predicted errors, which verifies the validity of the computed detector position errors.

CONCLUSIONS

It is possible to calibrate the detector positions in the SPOT CCD arrays without an external test field. A method was developed that uses simultaneously recorded overlapping images from the two sensors. Extracted information on differences between the images can be used to solve for the detector position errors as a function of detector number.

Applying the method to the panchromatic sensor in the SPOT-1 satellite revealed significant errors in the positions of detectors in the CCD arrays. These were close to the values from preflight tests, but still large enough to introduce systematic errors when using SPOT images for DTM computations. The solution gave a detailed description of detector position errors along the arrays. By using this information to correct SPOT imagery before stereo processing, it is possible to eliminate systematic errors in the computed elevations.

REFERENCES

Bjerhammar, A., 1971. Non-gaussian estimation. *Svensk Lantmäteritidskrift*, Vol. 64, No. 5–6, pp. 353–376.

Golub, G. H., and C. F. Van Loan, 1989. *Matrix Computations*. The John Hopkins University press. Baltimore and London. 642p.

Henry, C., A. Juvigny, and R. Serradeil, 1988. High Resolution Detection Assembly of the SPOT Camera: On-orbit results and Future Developments. *Acta Astronautica*, Vol. 17, No. 5, pp. 545–551.

Midan, J.P., 1986. The SPOT instrument performance: an overview of design and performance. *Earth-Orient. Applic. Space Technology*. Vol. 6, No. 2, pp. 163–172.

Rosenholm, D., 1987. Multi-Point Using the Least Squares Technique for Evaluation of Three-dimensional Models. *Photogrammetric Engineering & Remote Sensing*. Vol. 53, No. 6, pp. 621–626.

———, 1988. Multi-point matching along vertical lines in SPOT images. *Int. J. Remote Sensing*, Vol. 9, No. 10–11, pp. 1687–1703.

Westin, T., 1990. Precision Rectification of SPOT Imagery. *Photogrammetric Engineering & Remote Sensing*. Vol. 56, No. 2, pp. 247–253.

(Recieved 16 September 1991; accepted 15 January 1992)